




Optimisation of the net flow generated by artificial cilia performing tilted conical motion in confined micro-channels

Yiqing Sun^{1,2} , Tongsheng Wang^{1,2}, Tanveer ul Islam^{1,2}, Jaap den Toonder^{1,2} and Ye Wang^{1,2}

¹Department of Mechanical Engineering, Eindhoven University of Technology, 5600 MB The Netherlands

²Institute of Complex Molecular Systems, Eindhoven University of Technology, 5600 MB The Netherlands

Corresponding author: Ye Wang, y.wang2@tue.nl

(Received 4 March 2025; revised 5 July 2025; accepted 10 July 2025)

Cilia exist ubiquitously in nature, and they are very effective in generating flow in a low Reynolds number environment. Inspired by nature, various artificial cilia have been invented for microfluidic applications, and a nature-mimicking tilted conical motion was often used for flow generation due to its simplicity and effectiveness. However, the current theoretical model for predicting the net flow rate generated by the tilted conical motion fails when the cilia are in close confinement, i.e. when the tips of the cilia are close to the ceiling of their channel or chamber, which is, in reality, the most practical way to enhance flow rate generation. Moreover, numerical simulations are very expensive for optimisation of such designs. In this study, we derive a new theoretical model, taking into account the tilting and opening angles of the cone, the height of the chamber and the length of the cilia. The results differ significantly from when the ceiling is not considered, and counter-intuitively in some cases the flow can even reverse. These unexpected results have important implications for artificial cilium design and applications. We validate the model with both numerical simulations and experiments using magnetic artificial cilia, and show that the flow optimisation based on tilted conical cilium motion can now be performed accurately in a realistic and practical manner. This study not only offers a simple tool for optimising designs of artificial cilium-based systems for microfluidic applications, but it also provides fresh insights for understanding natural cilium-driven flows.

Key words: low-Reynolds-number flows, microfluidics, propulsion

1. Introduction

Cilia are microscopic hair-like organelles found ubiquitously in living organisms, and they perform various important biological functions (Ibañez-Tallon *et al.* 2003; Shinohara *et al.* 2012; Gilpin, Bull & Prakash 2020). There are two main types of cilia: motile and non-motile. Most non-motile cilia are primarily utilised for sensing (Wheway, Parry & Johnson 2014; Elliott & Brugmann 2019), while the motile cilia exhibit various mechanical functions by converting chemical energy into mechanical work. For example, cilia in the respiratory epithelium remove mucus-coated pathogens and inhaled particles from the airways (Bustamante-Marin & Ostrowski 2017). Some protozoa, such as *Paramecium*, use their oscillating cilia for propulsion and feeding (Bouhouche *et al.* 2022). Inspired by nature, various types of artificial cilia have been fabricated during the past decade. They can perform various functions such as mixing, particle transportation or flow generation (Fahrni, Prins & van IJzendoorn 2009; Zhou *et al.* 2015; Wang *et al.* 2016; Zhang *et al.* 2021). The most common means of actuation is by using magnetic fields, which allows untethered control and is compatible with biological substances. These magnetic artificial cilia are typically embedded in a closed microfluidic channel, and they are actuated with a rotating external magnetic field.

One of the most common types of artificial cilium motion can be described as a tilted conical motion, which was inspired by nature (Vilfan *et al.* 2010). This motion consists of an effective stroke, where cilia move more upright, dragging along more fluid, and a recovery stroke, where they move closer to the substrate, therefore less fluid flows backwards due to the proximity to the ‘floor’. This asymmetric motion results in a net flow being pumped in the direction of the effective stroke, and the flow rate has been shown to scale with $\sin \theta \sin^2 \varphi$ when the ceiling is far away from the cilium tip, with θ being the tilting angle of the axle and φ the opening angle of the cone (Smith, Blake & Gaffney 2008). For magnetic artificial cilia, this tilted conical motion can be realised using just a rotating magnet placed underneath the cilia, and a significant flow can be generated, up to an order of microlitres per minute (Wang *et al.* 2015).

A straightforward way to further optimise the flow is to increase the cilium length, making their tips even closer to the ceiling of the microfluidic channel. However, the relation of the flow to $\sin \theta \sin^2 \varphi$ fails when the hydrodynamic influence from the ceiling becomes significant, and to the knowledge of the authors, there is no theoretical model in the literature for the flow generated by the tilted conical motion where both the influence of the ceiling and the floor are included. Previous experiments (Evans *et al.* 2007; Shields *et al.* 2010; Kokot *et al.* 2011; ul Islam, Bellouard & den Toonder 2021), simulations (Kim & Netz 2006; Gauger, Downton & Stark 2009; Wei *et al.* 2021) and theories (Gauger & Stark 2006; Manghi, Schlagberger & Netz 2006; Vilfan & Jülicher 2006; Downton & Stark 2009) predominantly involve systems with the ceiling far away or without a ceiling, and therefore those results lack accuracy in predicting the real flow generation in microfluidic channels.

Because of the lack of a good theoretical model, flow generated by artificial cilia with a tilted conical motion in a channel is often only characterised by experimental observations, without being systematically optimised (Zhang *et al.* 2018; ul Islam *et al.* 2022). In addition, there are practical limitations to the cilium motion, i.e. the achievable tilting and opening angles of the cone, which are due to the limitations in the flexibility of the material, and the magnitude of the magnetic field. These limitations also need to be considered while optimising the design of the channel and the implementation of artificial cilia, especially for practical applications.

In this paper, we derive a new theoretical model for calculating the net flow generated by cilia moving in a tilted conical motion between two parallel plates, and we validate the model with both numerical simulations and experiments using magnetic artificial cilia

in a microfluidic channel. Furthermore, we show that the generated flow can be optimised using the theoretical model under various practical conditions and limitations, by changing the parameters including the cilium length, channel height and the tilting and opening angles of the cone. Interestingly, a counter-intuitive flow opposite to the ‘effective stroke’ direction can be generated under common experimental conditions. This phenomenon is fully captured by the theoretical model, and it turns out that such ‘reverse flows’ can even be beneficial for practical applications, for example in cases where there are limitations on the cilium motion when reducing the size of the actuator, and yet a large flow is required for applications such as fluid and particle transport (Park *et al.* 2023), or antifouling (Zhang *et al.* 2020). This work provides fresh insights for understanding the flow generation mechanism of the tilted conical cilium motion for both natural and artificial cilia, and it offers a simple tool for flow optimisation for artificial cilium applications.

2. Results and discussion

2.1. Theoretical model of the tilted conical motion generated net flow between two parallel plates

In order to generate net flow in a low Reynolds number environment, cilia typically need to perform a so-called non-reciprocal motion, which can be seen as a cyclical movement consisting of an effective stroke and a recovery stroke. In the tilted conical motion, the effective stroke is commonly considered to be half of the cycle where more fluid is transported in one direction, and the recovery stroke is the other half where less fluid is transported in the opposite direction, as shown in figure 1(a). Consequently, the net flow direction is usually consistent with the effective stroke direction.

A simplified conical rotation model was used to determine the optimal angular configuration that generates the maximum net flow (Nonaka *et al.* 2005). The position of point S on the cilia (x_S, y_S, z_S) with an arc length s from the root as function of time t can be prescribed as follows:

$$x_S(t) = s \sin \varphi \sin \omega t, \quad (2.1)$$

$$y_S(t) = s \cos \varphi \sin \theta - s \sin \varphi \cos \omega t \cos \theta, \quad (2.2)$$

$$z_S(t) = s \cos \varphi \cos \theta + s \sin \varphi \cos \omega t \sin \theta. \quad (2.3)$$

In this case, the cilia are seen as performing prescribed motions (tilted conical motion with a constant angular velocity), irrespective of the fluid drag, and they are assumed to tilt but not deform, i.e. they remain straight. This simplification has a practical root, since the magnetic artificial cilia typically experience a rather strong magnetic field, and the magnetic force dominates over viscous drag at moderate frequencies (typically under 30 Hz), which is evident from the fact that the amplitude of the motion of the cilia (cone opening angle) does not significantly decrease with the increase in actuation frequency using a permanent magnet. This also implies an almost linear frequency–flow rate relationship for easy control, which is convenient for applications. In addition, the cilia follow the external field generated by a rotating magnet, which typically has a constant angular velocity.

Based on the Green’s function for the flow generated by a Stokeslet near a no-slip plane (Blake 1971), Smith *et al.* (2008) derived the expression for the far-field net flow rate generated by cilia moving in such motion

$$Q = (1/6\pi\mu)C_N\omega L^3 \sin \theta \sin^2 \varphi, \quad (2.4)$$

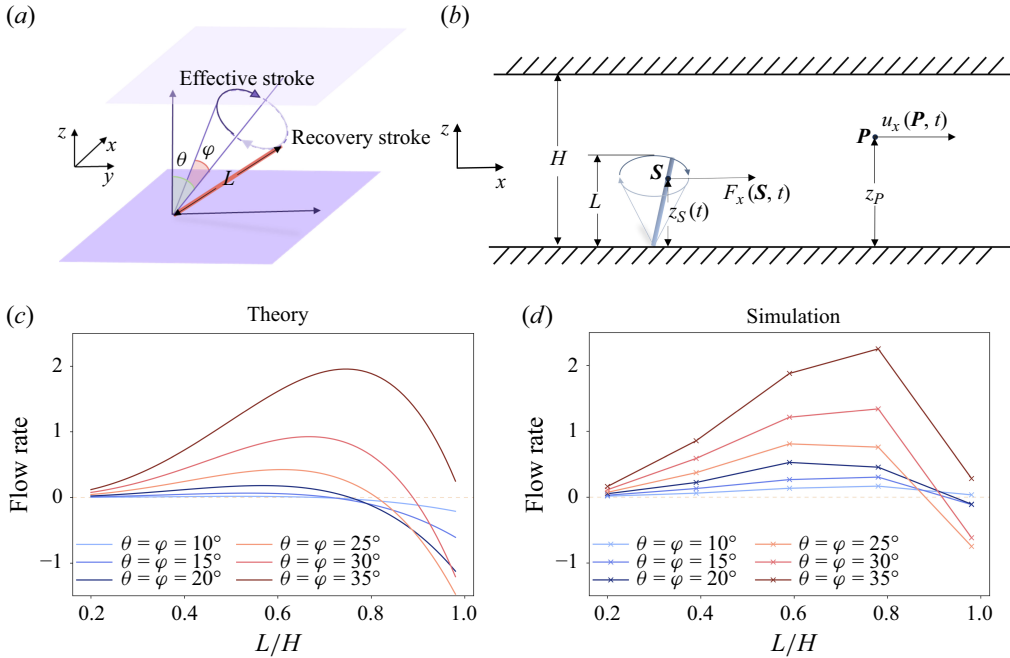


Figure 1. Theoretical model of cilium-generated flow by tilted conical motion between two parallel plates. (a) Schematic diagram of the rotation of a single cilium. Here, θ is the tilting angle, and φ is the opening angle of the cone. (b) Schematic of the side view. The model is derived from the Green's function for the fluid speed $u_x(P, t)$ at point P generated by a point force $F_x(S, t)$ on point S on the cilium. (c) The theoretical flow rate for different tilting and opening angles as a function of the length over channel height ratio L/H . We define $R_c C_N \omega / 12\mu$ arbitrarily as 100, and set $H = 1$. (d) Simulation results of the cilium-generated flow between two parallel plates, using COMSOL Multiphysics®.

where μ is the viscosity of the fluid, C_N is the resistance coefficient normal to the cilium length from the slender body theory (Gray & Hancock 1955), ω is the angular speed of the cilium rotation, L is the length of the cilia and θ and φ are the tilting and opening angles of the cone, respectively.

It can be seen that the generated net flow should scale with $\sin \theta \sin^2 \varphi$, which was also experimentally observed in relatively large chambers (Vilfan *et al.* 2010; Wang *et al.* 2015). However, these earlier experimental studies focused on developing fabrication methods of magnetic artificial cilia and experimentally validating their pumping capabilities, hence they did not consider the optimisation of the flow rate for actual microfluidic applications where flow must be generated in confined channels and chambers, which only started to emerge in recent years (Gu *et al.* 2020; Zhang *et al.* 2020; ul Islam *et al.* 2022).

For the optimisation of the flow generation using artificial cilia in a confined microfluidic channel, the aforementioned theoretical model (2.4) is no longer sufficient. The reason is that it does not take into account the upper no-slip boundary, or the ceiling of the channel in practice, which is important when longer cilia are used for generating larger flows. The benefit of using longer cilia can be easily appreciated from (2.4), where Q scales with L^3 . We will later show that the scaling law is no longer true when the tip of the cilia is close to the ceiling of the channel, but using longer cilia is still advantageous.

To obtain a net flow generated by tilted conically rotating cilium in a closed channel (figure 1b), we start with the results derived by Liron & Mochon (1976) for a Stokeslet between two parallel plates. The governing equations can be written as follows:

$$\nabla p = \mu \nabla^2 \mathbf{u} + \mathbf{F} \delta(\mathbf{P} - \mathbf{S}), \quad (2.5)$$

$$0 = \nabla \cdot \mathbf{u}, \quad (2.6)$$

where p is the pressure, μ is the fluid viscosity, \mathbf{F} is the point force at \mathbf{S} and $\delta(\mathbf{P} - \mathbf{S})$ is the Dirac delta function. With two no-slip boundaries at $z = 0$ and $z = H$, the resulting Green's function from (2.5) and (2.6) for a Stokeslet is derived by Liron & Mochon (1976) (see Supplementary material is available at <https://doi.org/10.1017/jfm.2025.10486>). Ignoring the terms that describe flow speeds orthogonal to the net flow direction (x) in the far field, the velocity at point \mathbf{P} can be expressed as

$$u_x(\mathbf{P}, t) \sim \frac{3H}{2\pi\mu} \frac{z_P}{H} \left(1 - \frac{z_P}{H}\right) \frac{z_S(t)}{H} \left(1 - \frac{z_S(t)}{H}\right) \frac{1}{D^2} \cdot F_x(\mathbf{S}, t), \quad (2.7)$$

where H is the height of the channel, z_P is the distance from point \mathbf{P} to the bottom plate, $z_S(t)$ is the distance from the point \mathbf{S} on the cilia to the bottom plate, D is the distance between \mathbf{S} and \mathbf{P} in the x direction and $F_x(\mathbf{S}, t)$ is the effective point force per unit length acting at point \mathbf{S} in the x direction at time t , and it scales with the speed of that point in the x direction.

Note that we only take the term from the original Green's function (Liron & Mochon 1976) that describes the generated flow parallel to the net flow direction (x) from the corresponding components of the source motion, while ignoring other terms that decay faster with the distance to the source. This is a reasonable simplification since we are interested in the net pumping rate inside a long microfluidic channel, in which the cilium patch typically occupies only a small portion of the total length of the channel.

When a cilium is performing tilted conical motion, the generated net fluid displacement over a cilium motion cycle at \mathbf{P} can be derived by integrating (2.7) along the length of the cilium, and over the cycle

$$v_x^{cilium, cycle}(\mathbf{P}) = \int_0^{\frac{2\pi}{\omega}} \int_0^L u_x(\mathbf{P}, t) ds dt. \quad (2.8)$$

It is important to note that, for any localised collection of point forces between infinitely large parallel plates, the net flow produced is zero (Liron & Mochon 1976). A finite flow rate, as observed in experiments, is a result of additional boundary conditions, and within a finite channel, a stable, parabolic flow profile develops over a short distance from the cilium patch (Wang *et al.* 2024). We assume that, in the practical case of a finite width of the channel, the dependency of the net velocity (and hence the flow rate) on the cilium motion is the same as that of the velocity of the infinite-plate case (later we show that this assumption is confirmed by the good agreement between theory and simulation).

It can be seen that u_x is parabolic along the z axis with a fixed source, and for the flow rate calculation, we can simplify the expression by first integrating the flow speed along the height of the channel, i.e. integrate $(z_P/H)(1 - (z_P/H))$ from 0 to H , resulting in $H/6$. And for a stable channel flow with a constant cross-section, the velocity at any point in the cross-section of the channel is invariant to the distance from the source when $D \gg H$. Therefore, the net flow rate can then be expressed as

$$Q = \frac{R_c \omega H^2}{4\pi\mu} \int_0^{\frac{2\pi}{\omega}} \int_0^L \frac{z_S(t)}{H} \left(1 - \frac{z_S(t)}{H}\right) F_x(\mathbf{S}, t) ds dt, \quad (2.9)$$

where we use a prefactor R_c to account for both the influence of the sidewalls on the magnitude of the (net) velocity and the fact that the flow rate scales linearly with the velocity (at any point in the channel). Here, ω is the angular velocity of cilium rotation

and F_x is the force in the x direction per unit length along the cilia. We ignore F_y and F_z because their contribution to the flow decays faster than F_x in the far field (Liron & Mochon 1976), and their effects cancel out over the cycle. Here, hydrodynamic interactions between the cilia are ignored, since the magnetic cilia cannot be closely packed, unless they are specifically designed to limit magnetic interaction (Wang *et al.* 2024). In the following analysis and comparisons with simulations and experiments, we treat R_c as a fitting parameter that can be considered as a measure of the influence of the boundary conditions on the averaged (and normalised) flux per channel height, and it is invariant to the motion of the cilia, but depends only on the geometry of the channel and the number of cilia.

The parameter F_x can be calculated using the theory developed first by Gray & Hancock (1955) for flagellum modelling, which treats them as slender bodies with hydrodynamic forces applied per unit length proportional to their speed with linear coefficients: C_N in the normal direction and C_T in the tangential direction with respect to the direction of the segment. Since in the model, the cilia always move normal to the length (Smith *et al.* 2008)

$$F_x(\mathcal{S}, t) = C_N \frac{dx_S(t)}{dt} = C_N s \omega \sin \varphi \cos \omega t. \quad (2.10)$$

In a practical sense, the velocity of any point on the cilia, and thus also the force applied by the cilia, increases linearly from the base to the tip at any given time, while F_x is tangent to the cone plane and its magnitude depends on the current angle of the cilia and is hence time dependent.

Substituting (2.3) and (2.10) into (2.9), we finally obtain (more details in the Supplementary Information)

$$Q = \frac{R_c C_N \omega L^3 H}{12\mu} \left(\sin \theta \sin^2 \varphi - \frac{3L}{2H} \cos \theta \cos \varphi \sin \theta \sin^2 \varphi \right). \quad (2.11)$$

The second term in the brackets in (2.11) brings an interesting property to the net flow generated. If the fitting parameter R_c takes a value of $2/\pi H$, and the length of the cilia is much smaller than the height of the channel ($L \ll H$), the second term in brackets becomes 0, and the result is equivalent to (2.4), where the flow scales with L^3 . However, as shown in figure 1(c), with a fixed H , the flow rate initially increases with L but reaches a peak at certain L/H values for given θ and φ and then decreases. Interestingly, the flow can even reverse to the opposite direction when the length of the cilia is greater than 80 % of the channel height for cilia rotating with relatively small opening and tilting angles (approximately 30° or less). This ‘reverse flow’ phenomenon is highly relevant experimentally and can even be utilised in practice, because the bending angles of the cilia always have practical limits, as we show in the supplementary information.

The scaling between the flow rate and the cilium configurations, as predicted by the model, is first validated by numerical simulation using COMSOL Multiphysics, as shown in figure 1(d), before being applied for optimisation and experimental validations. The numerical model has one cilium that performs a tilted conical motion between two parallel plates. The flow rate is measured by integrating quasi-static flows from different time points during a motion circle (see supplementary information for details). The theoretical and numerical results of figures 1(c) and 1(d) are in good agreement.

Note that the value of the prefactor (R_c) depends only on the geometry of the channel. Therefore, using this model can also help to obtain the exact flow rate in any channel configuration more efficiently. Since we now have verified the scaling behaviour of the theoretical expression, in principle, one only needs to run one full simulation for the exact

flow rate for one specific condition of cilium length/rotation angles, and the result for all other conditions can be obtained through simple scaling. This will save a significant amount of computation time.

These characteristics of the flow generated by the tilted conical motion, which were not discussed in any of the previous literature known to us, have profound implications for the practical application of artificial cilia. Indeed, we have been conducting research on magnetic artificial cilia for over a decade and have only recently encountered reverse flow when optimising the design of a cilium chamber for a practical application. We initially thought it was an experimental artefact and only later discovered the mechanism by performing the theoretical analysis reported here. For many researchers working on applications of artificial cilia, or even for people studying natural cilia, this model can provide guidance and valuable insight, as will be shown below with some examples.

2.2. Optimisation of cilium-driven flow

We can now use (2.11) to optimise cilium-generated flow in various practical scenarios. We have already shown in figure 1(c) the effect of increasing the cilium length with a set cone opening angle φ , while the tilting angle $\theta = \varphi$. In reality, one can change θ and φ independently (for a tilted conical motion generated by a rotating permanent magnet, which is positioned underneath or above the cilia array with its rotation axis normal to the substrate (Shields *et al.* 2010; Wang *et al.* 2016; Zhang *et al.* 2018), θ is mainly determined by the in-plane (cilium substrate) offset of the rotation axis to the cilia, and φ is determined by a combination of factors, mainly the strength of the magnet, the distance between the magnet and the cilia in the out-of-plane direction and the radius of rotation. For the same motion generated by an electromagnet (Wang *et al.* 2013, 2015), the angles can be adjusted by changing the time-dependent field strength from different poles. For both actuation methods, at high frequencies, these angles can decrease due to hydrodynamic drag and inductance (for an electromagnet)) and the effect is shown in figure 2. When H is fixed, for moderate θ and φ values ($< 30^\circ$), significant ‘reverse’ flow can be obtained (figure 2a,b) when the cilia can almost touch the ceiling of the channel ($L/H = 0.98$), with the magnitude reaching its peak around $\theta = 22^\circ$ and $\varphi = 29^\circ$. In contrast, cilia that are half the height of the channel (figure 2c,d) generate positive but lower flow rates with θ and φ smaller than $< 30^\circ$, which increases monotonically with θ and φ .

The results shown in figure 2 are important for practical applications, as most of the tilted conical motions performed by magnetic artificial cilia do not have large tilting and opening angles (Fahrni *et al.* 2009; Venkataramanachar *et al.* 2023). We have also measured the bending angles of cilia used in the experimental part of this study (as reported below), and the results show that they do not exceed 50° in a practical set-up (meaning that the maximum θ and φ can be approximately 25°), see Supplementary Data. It can be observed from figure 2, that, for these moderate but practical values of θ and φ (a cone that opens at a sharp angle and is moderately ‘tilted’), a practical way of maximising the flow rate is to choose a large cilium length L and utilise the ‘reverse’ flow, which can be more effective than trying to maximise the flow in the traditional ‘effective stroke’ direction.

If we disregard the practical limitation in the achievable cone angles, theoretical maximum flow rates can be calculated for various L/H , as shown in figure 3(a). For comparison, we have also plotted as dotted lines the result from (2.11) without the second term, which is equivalent to (2.4) with a different scaling factor. The two equations should not be compared in terms of absolute values, since (2.4) is the flow rate in semi-infinite space and cannot be directly used to calculate the flow rate in a channel without proper scaling.

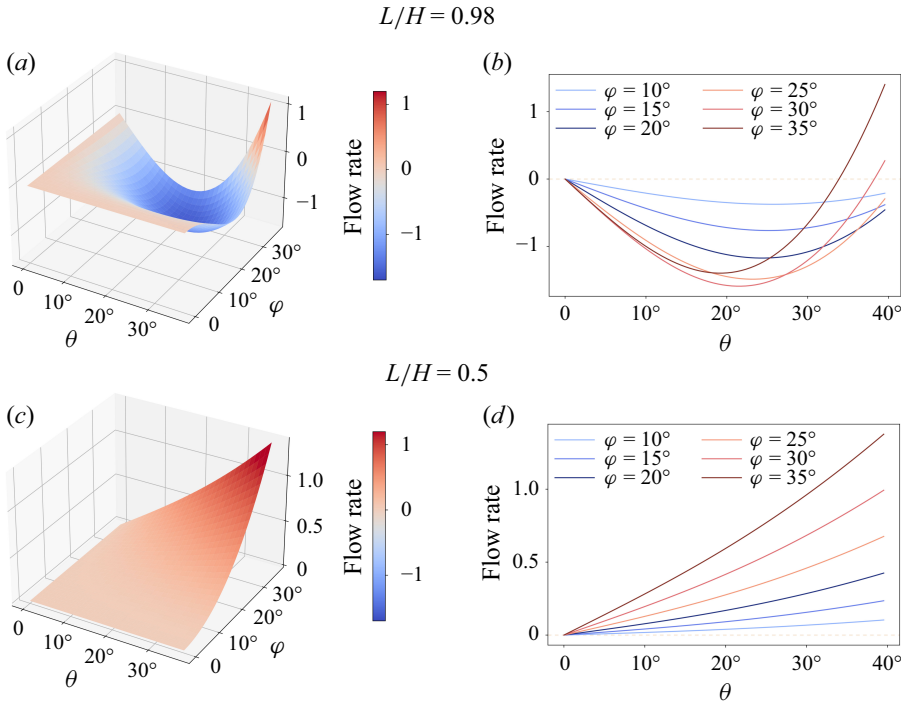


Figure 2. The influence of the tilting and opening angles θ and φ on cilium-generated flow at different L/H ratios. We define $R_c C_N \omega / 12 \mu$ arbitrarily as 100, and set $H = 1$. (a) The three-dimensional graph at $L/H = 0.98$ shows the magnitude of the reverse flow caused by the hydrodynamic influence from the ceiling; (b) two-dimensional cross-sections of the data showing the relation between the flow rate and θ at different φ , for $L/H = 0.98$; (c) the three-dimensional graph of cilium-generated flow at $L/H = 0.5$ for different θ and φ , showing no reverse flow; (d) two-dimensional cross-sections of the data showing the profile of flow rate with θ for different φ , for $L/H = 0.5$.

To reach the maximum net flow, the ‘recovery stroke’ should ‘touch’ the floor, meaning that $\theta + \varphi = 90^\circ$, as illustrated in figure 3(b). Applying (2.11), figure 3(a) shows that when the recovery stroke is close enough to the floor, no more ‘reverse flow’ can occur for any L/H values. With relatively small L/H , the flow rate follows a trend similar to (2.4) of the single boundary case, with the peak close to $\varphi = \arctan(\sqrt{2}) = 54.7^\circ$ (Smith *et al.* 2008; Downton & Stark 2009). With increasing L/H , the angle φ at which the flow reaches maximum deviates further from the single boundary scenario. The maximum ‘forward flow’ is achieved when $L = H$ (assuming that the length of cilia does not exceed the height of the channel) at $\varphi = 70.9^\circ$ (see Supplementary Data for details).

Note that, for very large L/H , a rather flat plateau emerges between 30° and 40° , because the benefit of a larger opening angle of the cone is practically cancelled out by the increase in drag when the cilia move closer to the upper ceiling. This plateau can be useful for practical applications, when a larger opening angle of the cone is hard to obtain. Furthermore, small variations in flow rate within a relatively wide range of angles can be beneficial for closed-loop control of the flow by providing a window of operation with a stable outcome. This can be particularly interesting for controlling the flow rate by the actuation frequency, as an increase in frequency results in a decrease in cone opening angle due to the increased hydrodynamic drag, which results in the flow rate generated increasing less than linearly with frequency (Wang *et al.* 2015). The plateau can help mitigate this effect for a more predictable outcome.

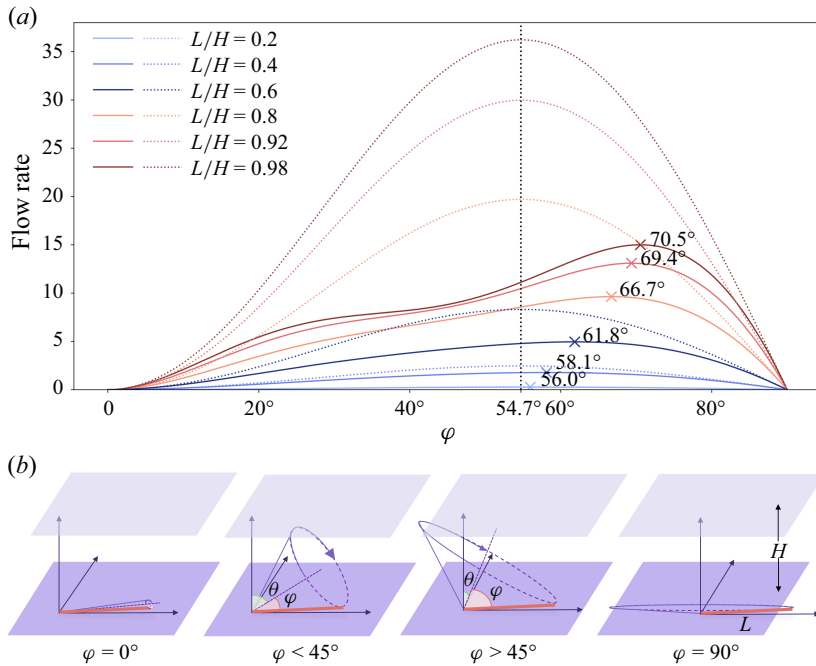


Figure 3. Theoretical maximum flow generation with tilted conical motion, when the cone opening angle and the channel height are fixed. Here, $R_c C_N \omega / 12 \mu$ is also arbitrarily defined as 100, and $H = 1$. (a) The change of cilium-generated flow with respect to φ and L/H . Here, θ is under the condition of $\theta + \varphi = 90^\circ$. The flow reaches maximum values at different φ for different L/H as indicated in the graph; for comparison, results from the single plane model (equivalent as (2.11) without the second term) are also plotted as dotted lines. (b) Schematic demonstrations of cilium movement under the condition of $\theta + \varphi = 90^\circ$. Note that the lowest point of the motion touches the floor, for minimisation of the flow from the recovery stroke, hence maximising the total net flow.

In practice, one can make the equilibrium angle of the cilia at rest (zero elastic bending) be at an angle θ to the normal of the substrate, using special techniques such as micromoulding (Broeren *et al.* 2023; Wang *et al.* 2024), which makes it easier for the cilium motion to obtain larger cone opening angles without needing an excessively large magnetic field. These parameters can be customised for different microfluidic channels to achieve optimised net flow in terms of both magnitude and reliability. The theoretical model presented above can thus be used to make informed design choices for these systems.

2.3. Experimental validation of the theoretical model

In order to validate the model, we have carried out a series of experiments using magnetic artificial cilia. The cilia were made using a method reported earlier (Cui *et al.* 2023), see figure 4(a). In short, a mould containing cavities for a 7×10 cilium array (cilium height is 320 μm , diameter is 35 μm , pitch is 350 μm) was first made out of fused silica using a femtosecond-laser-assisted-etching (FLAE) technique, followed by transfer moulding of a magnetic polymer mixture consisting of iron powder and poly (styrene-block-isobutylene-block-styrene) (SIBS) using a hot-embossing set-up. After cooling, the cilium patch was demoulded and integrated into a microfluidic chip also made with FLAE for precise geometries. The bottom part of the chip has a recirculatory channel with a height of 300 μm and a width of 3 mm, and an additional 100 μm recess is present in the

cilium patch area to compensate for the thickness of the cilium substrate. The upper part features two fluid inlets and a matching recess area that defines the channel height of the cilium chamber (figure 4b,c). The amount of recess is varied in different experiments (figure 4e). Finally, the whole device was sealed using a low viscosity epoxy glue (Araldite 2020), leaving only two ports for fluid filling. Inlets were sealed with adhesive tapes after filling the device with fluid, using water with tracer particles (monodisperse COOH functionalised polystyrene particles, 10 % w/v aq., microParticles GmbH) at a concentration of 0.12 vol %.

The cilia can be magnetically actuated using a set-up developed in an earlier study (figure 4d) (ul Islam *et al.* 2021). In the set-up, a permanent neodymium magnet (disc magnet 8×8 mm, N48, Magnetenspecialist) is fixed to a rotating head. The head is positioned underneath the microfluidic chip containing the cilium array, with the rotation axis positioned 3 mm away from the centre of the cilium patch in the direction normal to the sidewalls. Rotation of the magnet then results in a tilted conical motion of the cilia with the tilting axis in the cross-sectional plane of the channel, therefore directing the net flow along the main axis of the channel (figure 4g). The cone opening (φ) and tilting (θ) angles were measured using images taken by a digital camera (PHANTOM VEO 1310 L-model camera) through an optical microscope (Olympus BX51), and φ was revised by adjusting the vertical distance between the magnet and the cilium patch (with θ as close to φ as possible), and was fixed at 17.5° in order to obtain a large flow. The net flow generated by the movement of the cilia was measured by tracing the suspended particles half-way through the recirculatory part of the channel (figure 4f), where the flow speed has fully developed into a stable profile. The total flow rate is calculated by measuring the flow speed at the centre point of the cross-section and using the theoretical expression for the flow profile in a rectangular channel (White & Majdalani 2006; Bruus 2007).

Figure 4(h) shows the effect of changing L/H on the net flow generated. The experimental result matches well with the trend predicted theoretically. Note that, in order to maintain the shape of the tilted conical motion, the height of the cilia L was fixed and only H was varied on different chips to vary L/H . This is different from the earlier theoretical analysis, where H was fixed and L varied. As the dimension was fixed for most part of the channel across different experiments, $R_c C_N \omega L^3 H / 12\mu$ can be treated as a fixed value ($31.5 \mu\text{l min}^{-1}$, as a result of applying least square fit to the experiment and numerical data). As shown in figure 4(h), when L/H was increased, the flow rate gradually increased until it reached a maximum value around $L/H = 0.5$. As L/H increased further, the flow rate decreased and reversed to the opposite direction, against the effective stroke due to the effect of the upper ceiling, as predicted by theory. The maximum opposite flow observed in the experiment is approximately five times that of the maximum achievable positive flow in the previously considered ‘effective stroke’ direction, even after optimising θ and φ by tuning the magnetic actuation set-up (both 17.5°).

In the experiments, the cilia are placed in a $350 \mu\text{m}$ pitch grid. As explained earlier, the hydrodynamic interactions do not influence the cilium motion to a significant degree (since the magnetic force dominates). However, neighbouring cilia can potentially influence each other’s flow field, as they have finite volume, while the model treats them as singularities. To get a sense of the order of magnitude of the influence, one may consider the volume occupied by the cilia compared with the total volume of the region. The cilia have a diameter of $35 \mu\text{m}$ and a length of $350 \mu\text{m}$, so they occupy less than 0.01 % of the fluid volume. However, this can be very different when the cilia are very closely packed. Our recent work (Wang *et al.* 2024) on closely packed metachronal cilium arrays shows that the intercilium hydrodynamics can effectively generate flow when they are sufficiently close together with a phase-modulated symmetry-breaking effect (the gap was approximately

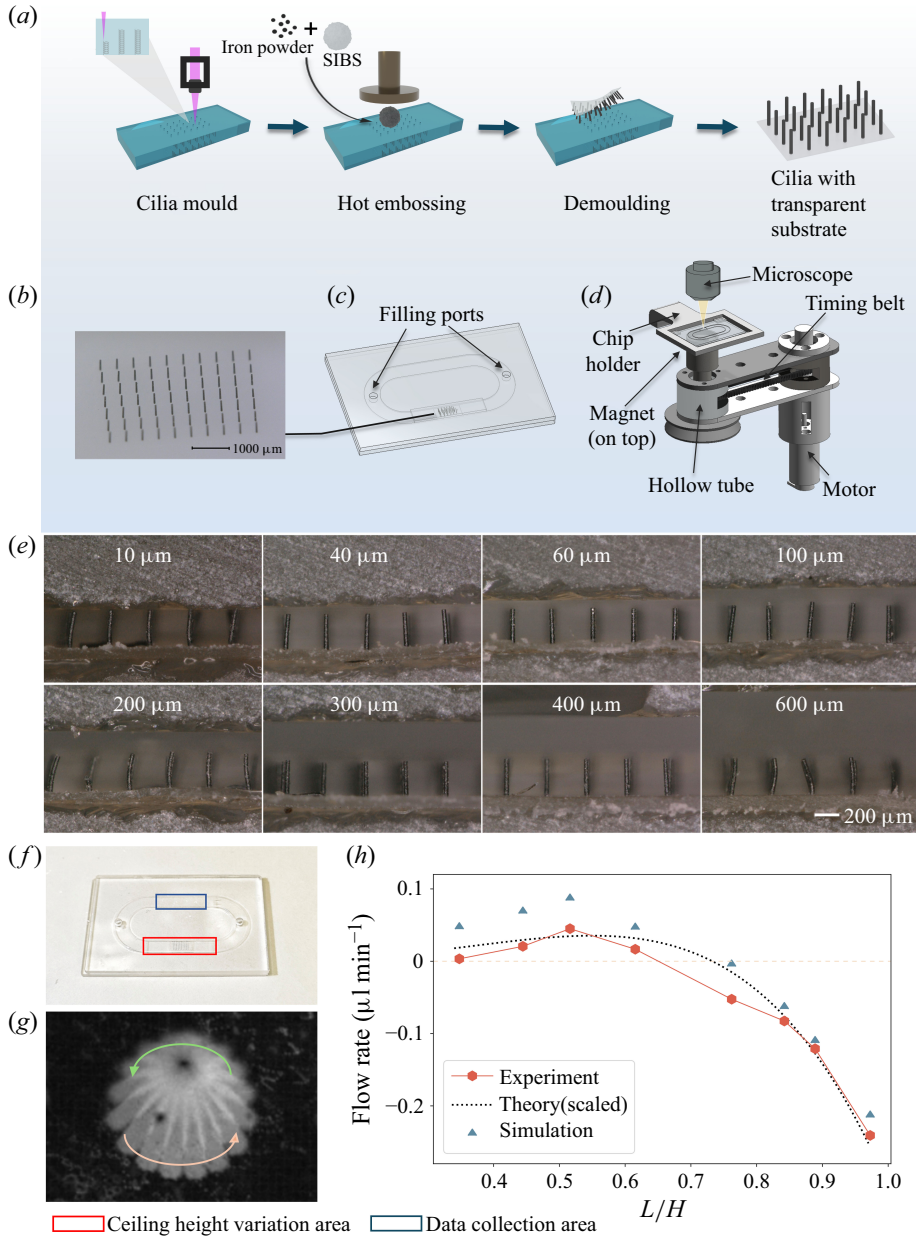


Figure 4. Experimental set-up and results for validation of the theoretical model. (a) The fabrication process of cilium arrays with a transparent substrate; (b) microscopy image of a 7×10 array of cilia, length $320 \mu\text{m}$, diameter $35 \mu\text{m}$ and pitch $350 \mu\text{m}$; (c) schematic drawing of the channel with integrated cilium patch; (d) magnetic actuation set-up with the chip holder; (e) side view images of cilia in channels of different heights. The distances from the cilium tips to the ceilings are 10 , 40 , 60 , 100 , 200 , 300 , 400 and $600 \mu\text{m}$, respectively; these images were taken after cutting the microfluidic chips in a straight line next to the edge of the cilia patch. (f) The assembled chip with a cilium array. The cap was etched only partially above the cilia (red rectangle) to vary the channel height. The blue rectangle indicates the location of the flow measurement; (g) top view image of one rotating artificial cilium showing the tilted conical motion, composed of 25 frames in one actuation cycle. The green arrow indicates the effective stroke, and the orange arrow indicates the recovery stroke; (h) the generated flow rate and pressure drop at different L/H . The red line represents the experimental results, the blue triangles represent the simulation results and the black dashed line represents the fitted theoretical calculations. The flow rates were measured at 600 RPM .

1/5 of their length, and those cilia were shaped like flaps, so the volume percentage was approximately 5 %).

3. Conclusions and outlook

We have derived a theoretical model to calculate the net flow generated by artificial cilia that perform a conical motion tilted in confined microfluidic channels. In this model, the influence of the channel ceiling on the flow is taken into account and the resulting scaling behaviour between the generated flow and the cilium configurations differs significantly from the earlier model that ignored this influence. We also performed experiments and numerical simulations, and both of the resulting net flow rates obtained from the experiments and simulations agree well with the theoretical prediction. Interestingly, certain non-trivial and practically relevant conditions can unexpectedly generate significant flow in the opposite direction to the commonly believed ‘effective stroke’ direction of the cilium motion, due to the influence of the channel ceiling.

The model can be used to optimise the performance of artificial cilia in existing systems and to create optimal designs within practical boundary conditions. For example, we have shown that when using magnetic artificial cilia actuated with a rotating magnet, the ‘reverse’ flow can be much stronger than attainable ‘positive’ flows, and the model perfectly captures this phenomenon.

On the one hand, the insights obtained from our study suggest a fundamental re-assessment in designing and using artificial cilia for practical applications. Cilium-based *in situ* microfluidic pumps can be made more effective beyond the current state of the art, especially when combined with newly developed micro-moulding techniques and new materials (ul Islam *et al.* 2022; Wang *et al.* 2024). Since the generated flow can now be quickly and reliably predicted, optimised and controlled, this design tool can stimulate the broader adoption of artificial cilium technology in a wider range of applications, including rapid diagnostics, lab-on-a-chip, organs-on-a-chip and micro-robotics. On the other hand, the results of this study could help in studying the behaviour of natural cilia, especially when they operate within close boundaries, such as in the embryonic node (Lee & Anderson 2008). The new insights could help to achieve more precise analysis of the effectiveness and efficiency of these wonderful organelles.

4. Materials and methods

4.1. Simulation of fluid flow generated by a single cilium

We developed a three-dimensional (3-D) simulation model in COMSOL Multiphysics® to calculate the net flow generated by a single cilium for different ratios of channels L/H (figure 1*d*). In the model, the tiled conical motion of the cilium was prescribed by adding a rotating domain containing a no-slip boundary as the surface of the cilium (frozen rotor application). The fluid inertia was ignored, and the full cilium motion was separated into several quasi-static snapshots. The governing equations are

$$0 = \nabla \cdot \boldsymbol{\sigma} + \boldsymbol{f}, \quad (4.1)$$

$$0 = \nabla \cdot \boldsymbol{u}, \quad (4.2)$$

where $\boldsymbol{\sigma}$ is the sum of fluid stresses, \boldsymbol{f} is the external force and \boldsymbol{u} is the fluid velocity. To minimise the influence of sidewalls, the channel in the model has a width of 10 mm. The channel length was set at 10 mm, which is significantly greater than the channel height, which was set at 1.02 mm. The diameter of the cilium was set at 10 μm . A no-slip boundary condition was set on the sidewalls and on the top and bottom walls of

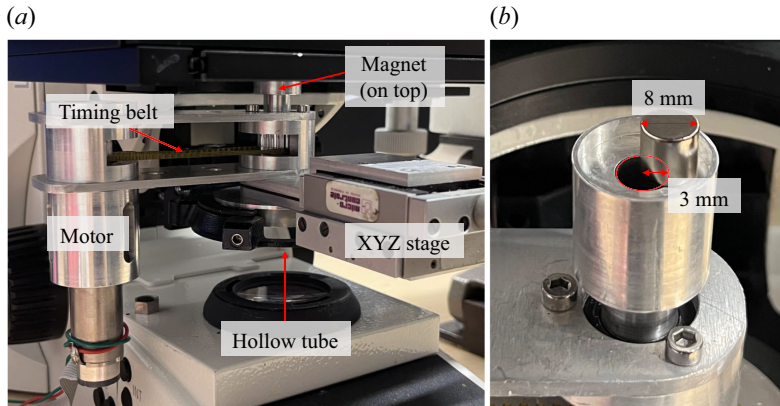


Figure 5. (a) Magnetic actuator set-up for actuating the artificial cilia for flow visualisation on a microscope. The set-up was developed in an earlier study (ul Islam *et al.* 2021). (b) Zoomed-in view of the rotating head with an off-centred magnet for generating a tilted conical motion on the cilia.

the channel, while the inlet and outlet were configured as open boundaries. Quasi-static simulations were performed on snapshots during the full cycle at equally spaced angles (20° pitch). Afterwards, the flow velocities were derived from these snapshots in a cross-section close to the inlet. The velocities from different time points in one motion cycle were integrated over time and the cross-sectional area to obtain the net flow rate over one cycle.

4.2. Simulation of fluid flow generated by an array of cilia

We developed a 3-D simulation model using ANSYS Fluent to study the effect of channel height on net flow generation by an array of cilia. The cilium motion was prescribed as a titled conical motion, and a moving mesh was used to implement the cilium rotation. Since ANSYS Fluent employs the finite volume method rather than the finite element method used in COMSOL, the computational resource requirement is significantly reduced when solving large 3-D problems. In the Fluent model, we solved the Navier–Stokes equations without incorporating turbulence models

$$\nabla \cdot \mathbf{u} = 0, \quad (4.3)$$

$$\rho \left(\frac{\partial \mathbf{u}}{\partial t} + \mathbf{u} \cdot \nabla \mathbf{u} \right) = -\nabla p + \mu \nabla^2 \mathbf{u}, \quad (4.4)$$

where \mathbf{u} is the fluid velocity vector, ρ is the fluid density, t is time, p is the fluid pressure and μ is the dynamic viscosity of the fluid. The computation domain is the same as the experimental set-up, and we measure the net flow at an interior cross-section at the data collection area, as shown in figure 4(f).

4.3. Magnetic actuator

The complete magnetic actuator features a rotating head connected to a motor with a timing belt, as shown in figure 5. The rotating head is equipped with a neodymium magnet (N48 disc magnet with 8 mm diameter and 8 mm height), allowing it to perform a controlled rotation with a distance from the centre of the magnet to the rotation axis of 3 mm (figure 5b). A controller that connects to a computer and the actuator is used to control the rotational frequency of the rotating head. A manual xyz stage is used to position the actuator to obtain optimal cilium motion.

4.4. Experimental measurement of the flow

Water with a suspension of 5 μm polystyrene microspheres was injected into the circular channel through one of the inlets. The channel was placed over the actuator. A microscope (Olympus BX51) equipped with a high-speed camera (PHANTOM VEO 1310 L-model camera) was used to visualise the motion of artificial cilia. We adjusted the relative position between the cilia and the magnet to achieve optimal cilium motion. After that, the movement of the particles in the channel was tracked with the high-speed camera. The focal plane of the microscope was adjusted to be in the centre of the channel height to measure the flow velocity, and the theoretical expression for the flow profile in a rectangular channel was used to calculate the flow rate (White & Majdalani 2006; Bruus 2007).

Supplementary material. Supplementary material is available at <https://doi.org/10.1017/jfm.2025.10486>.

Acknowledgements. The authors thank EPC (Equipment and Prototype Center) at TU/e for the fabrication of the actuation set-up.

Funding. This work is supported by the European Union's Horizon 2020 research and innovation program under grant agreement No 953234, project Tumor-LN-oC.

Declaration of interests. The authors report no conflict of interest.

Author contributions. Yiqing Sun and Ye Wang designed and performed research and analysed data; Tanveer Ul Islam designed the magnetic actuator; Tongsheng Wang developed the ANSYS model; Ye Wang developed the COMSOL model; Ye Wang and Jaap den Toonder provided the resources and reviewed the manuscript; all authors contributed to the original manuscript.

REFERENCES

- BLAKE, J.R. 1971 A note on the image system for a stokeslet in a no-slip boundary. *Math. Proc. Camb. Phil. Soc.* **70** (2), 303–310.
- BOUHOUCHE, K., VALENTINE, M.S., LE BORGNE, P., LEMULLOIS, M., YANO, J., LODH, S., NABI, A., TASSIN, A.M. & VAN HOUTEN, J.L. 2022 Paramecium, a model to study ciliary beating and ciliogenesis: insights from cutting-edge approaches. *Frontiers Cell Dev. Biol.* **10**, 847908.
- BROEREN, S., PEREIRA, I.F., WANG, T., DEN TOONDER, J.M.J. & WANG, Y. 2023 On-demand microfluidic mixing by actuating integrated magnetic microwalls. *Lab Chip* **23** (6), 1524–1530.
- BRUUS, H. 2007 *Theoretical Microfluidics*. Oxford University Press.
- BUSTAMANTE-MARIN, X.M. & OSTROWSKI, L.E. 2017 Cilia and mucociliary clearance. *Cold Spring Harb. Perspect. Biol.* **9** (4), a028241.
- CUI, Z., WANG, Y., ZHANG, S., WANG, T. & DEN TOONDER, J.M.J. 2023 Miniaturized metachronal magnetic artificial cilia. *Proc. Natl Acad. Sci. USA* **120** (35), e2304519120.
- DOWNTON, M.T. & STARK, H. 2009 Beating kinematics of magnetically actuated cilia. *Europhys. Lett.* **85** (4), 44002.
- ELLIOTT, K.H. & BRUGMANN, S.A. 2019 Sending mixed signals: cilia-dependent signaling during development and disease. *Dev. Biol.* **447** (1), 28–41.
- EVANS, B.A., SHIELDS, A.R., CARROLL, R.L., WASHBURN, S., FALVO, M.R. & SUPERFINE, R. 2007 Magnetically actuated nanorod arrays as biomimetic cilia. *Nano Lett.* **7** (5), 1428–1434.
- FAHRNI, F., PRINS, M.W.J. & VAN IJZENDOORN, L.J. 2009 Micro-fluidic actuation using magnetic artificial cilia. *Lab Chip* **9** (23), 3413–3421.
- GAUGER, E.M., DOWNTON, M.T. & STARK, H. 2009 Fluid transport at low Reynolds number with magnetically actuated artificial cilia. *Eur. Phys. J. E* **28**, 231–242.
- GAUGER, E. & STARK, H. 2006 Numerical study of a microscopic artificial swimmer. *Phys. Rev. E* **74** (2), 021907.
- GILPIN, W., BULL, M.S. & PRAKASH, M. 2020 The multiscale physics of cilia and flagella. *Nat. Rev. Phys.* **2** (2), 74–88.
- GRAY, J. & HANCOCK, G.J. 1955 The propulsion of sea-urchin spermatozoa. *J. Expl Biol.* **32** (4), 802–814.
- GU, H., *et al.* 2020 Magnetic cilia carpets with programmable metachronal waves. *Nat. Commun.* **11** (1), 2637.

- IBAÑEZ-TALLON, I., HEINTZ, N. & OMRAN, H. 2003 To beat or not to beat: roles of cilia in development and disease. *Hum. Mol. Genet.* **12** (suppl_1), R27–R35.
- UL ISLAM, T., BELLOUARD, Y. & DEN TOONDER, J.M.J. 2021 Highly motile nanoscale magnetic artificial cilia. *Proc. Natl Acad. Sci. USA* **118** (35), e2104930118.
- UL ISLAM, T., *et al.* 2022 Microscopic artificial cilia—a review. *Lab Chip* **22** (9), 1650–1679.
- KIM, Y.W. & NETZ, R.R. 2006 Pumping fluids with periodically beating grafted elastic filaments. *Phys. Rev. Lett.* **96** (15), 158101.
- KOKOT, G., VILFAN, M., OSTERMAN, N., VILFAN, A., KAVČIČ, B., POBERAJ, I. & BABIČ, D. 2011 Measurement of fluid flow generated by artificial cilia. *Biomicrofluidics* **5** (3), 34103–341039.
- LEE, J.D. & ANDERSON, K.V. 2008 Morphogenesis of the node and notochord: the cellular basis for the establishment and maintenance of left–right asymmetry in the mouse. *Dev. Dyn.* **237** (12), 3464–3476.
- LIRON, N. & MOCHON, S. 1976 Stokes flow for a stokeslet between two parallel flat plates. *J. Engng Maths* **10** (4), 287–303.
- MANGHI, M., SCHLAGBERGER, X. & NETZ, R.R. 2006 Propulsion with a rotating elastic nanorod. *Phys. Rev. Lett.* **96** (6), 068101.
- NONAKA, S., YOSHIBA, S., WATANABE, D., IKEUCHI, S., GOTO, T., MARSHALL, W.F. & HAMADA, H. 2005 De novo formation of left–right asymmetry by posterior tilt of nodal cilia. *PLoS Biol.* **3** (8), e268.
- PARK, S., CHOI, G., KANG, M., KIM, W., KIM, J. & JEONG, H.E. 2023 Bioinspired magnetic cilia: from materials to applications. *Microsyst. Nanoengng* **9** (1), 153.
- SHIELDS, A.R., FISER, B.L., EVANS, B.A., FALVO, M.R., WASHBURN, S. & SUPERFINE, R. 2010 Biomimetic cilia arrays generate simultaneous pumping and mixing regimes. *Proc. Natl Acad. Sci. USA* **107** (36), 15670–15675.
- SHINOHARA, K., KAWASUMI, A., TAKAMATSU, A., YOSHIBA, S., BOTILDE, Y., MOTOYAMA, N., REITH, W., DURAND, B., SHIRATORI, H. & HAMADA, H. 2012 Two rotating cilia in the node cavity are sufficient to break left–right symmetry in the mouse embryo. *Nat. Commun.* **3** (1), 622.
- SMITH, D.J., BLAKE, J.R. & GAFFNEY, E.A. 2008 Fluid mechanics of nodal flow due to embryonic primary cilia. *J. R. Soc. Interface* **5** (22), 567–573.
- VENKATARAMANACHAR, B.B., LI, J., UL ISLAM, T.L., WANG, Y. & DEN TOONDER, J.M.J. 2023 Nanomagnetic elastomers for realizing highly responsive micro-and nanosystems. *Nano Lett.* **23** (20), 9203–9211.
- VILFAN, A. & JÜLICHER, F. 2006 Hydrodynamic flow patterns and synchronization of beating cilia. *Phys. Rev. Lett.* **96** (5), 058102.
- VILFAN, M., POTOČNIK, A., KAVČIČ, B., OSTERMAN, N., POBERAJ, I., VILFAN, A. & BABIČ, D. 2010 Self-assembled artificial cilia. *Proc. Natl Acad. Sci. USA* **107** (5), 1844–1847.
- WANG, T., UL ISLAM, T., STEUR, E., HOMAN, T., AGGARWAL, I., ONCK, P.R., DEN TOONDER, J.M.J. & WANG, Y. 2024 Programmable metachronal motion of closely packed magnetic artificial cilia. *Lab Chip* **24** (6), 1573–1585.
- WANG, Y., GAO, Y., WYSS, H.M., ANDERSON, P.D. & DEN TOONDER, J.M.J. 2013 Out of the cleanroom, self-assembled magnetic artificial cilia. *Lab Chip* **13** (17), 3360–3366.
- WANG, Y., GAO, Y., WYSS, H.M., ANDERSON, P.D. & DEN TOONDER, J.M.J. 2015 Artificial cilia fabricated using magnetic fiber drawing generate substantial fluid flow. *Microfluid Nanofluid* **18**, 167–174.
- WANG, Y., DEN TOONDER, J.M.J., CARDINAELS, R. & ANDERSON, P.D. 2016 A continuous roll-pulling approach for the fabrication of magnetic artificial cilia with microfluidic pumping capability. *Lab Chip* **16** (12), 2277–2286.
- WEI, D., DEHNAVI, P.G., AUBIN-TAM, M. & TAM, D. 2021 Measurements of the unsteady flow field around beating cilia. *J. Fluid Mech.* **915**, A70.
- WHEWAY, G., PARRY, D.A. & JOHNSON, C.A. 2014 The role of primary cilia in the development and disease of the retina. *Organogenesis* **10** (1), 69–85.
- WHITE, F.M. & MAJDALANI, J. 2006 *Viscous Fluid Flow*. McGraw-Hill New York.
- ZHANG, S., CUI, Z., WANG, Y. & DEN TOONDER, J.M.J. 2021 Metachronal μ -cilia for on-chip integrated pumps and climbing robots. *ACS Appl. Mater. Interfaces* **13** (17), 20845–20857.
- ZHANG, S., WANG, Y., LAVRIJSEN, R., ONCK, P.R. & DEN TOONDER, J.M.J. 2018 Versatile microfluidic flow generated by moulded magnetic artificial cilia. *Sensors Actuators B: Chem.* **263**, 614–624.
- ZHANG, S., ZUO, P., WANG, Y., ONCK, P. & DEN TOONDER, J.M.J. 2020 Anti-biofouling and self-cleaning surfaces featured with magnetic artificial cilia. *ACS Appl. Mater. Interfaces* **12** (24), 27726–27736.
- ZHOU, B., XU, W., SYED, A.A., CHAU, Y., CHEN, L., CHEW, B., YASSINE, O., WU, X., GAO, Y. & ZHANG, J. 2015 Design and fabrication of magnetically functionalized flexible micropillar arrays for rapid and controllable microfluidic mixing. *Lab Chip* **15** (9), 2125–2132.